AUTHOR QUERY FORM

ELSEVIER	**Journal: MAMT** **Article Number: 1832**	**Please e-mail or fax your responses and any corrections to:** **E-mail: corrections.eseo@elsevier.spitech.com** **Fax: +1 619 699 6721**

Dear Author,

Any queries or remarks that have arisen during the processing of your manuscript are listed below and highlighted by flags in the proof. Please check your proof carefully and mark all corrections at the appropriate place in the proof (e.g., by using on-screen annotation in the PDF file) or compile them in a separate list.

For correction or revision of any artwork, please consult http://www.elsevier.com/artworkinstructions.

Any queries or remarks that have arisen during the processing of your manuscript are listed below and highlighted by flags in the proof. Click on the 'Q' link to go to the location in the proof.

Location in article	Query / Remark: click on the Q link to go Please insert your reply or correction at the corresponding line in the proof
Q1	Please check the telephone/fax number of the corresponding author, and correct if necessary.
Q2	Research Highlights should consist of only 125 characters per bullet point, including spaces. However, the research highlights provided for this item exceed the maximum requirement. Kindly provide the necessary corrections. For more information, please see Guide for Authors.
Q3	Closing parenthesis has been deleted. Please check, and correct if necessary.
Q4	”Figs. 15-d, 17-d and 17d” was changed to ”Figs. 15-d, 17-c and 17d”. Please check and amend as necessary.
Q5	Please provide journal title for references [5, 36].
Q6	Please provide journal title for references [5, 36].

Thank you for your assistance.

Mechanism and Machine Theory xxx (2011) xxx

Contents lists available at ScienceDirect

Mechanism and Machine Theory

journal homepage: www.elsevier.com/locate/mechmt

Highlights

Mechanism and Machine Theory xxx (2011) xxx–xxx

Vision/force control of parallel robots

S. Bellakehal [a,*], N. Andreff [a], Y. Mezouar [a], M. Tadjine [b]

[a] LASMEA-CNRS-Université Blaise Pascal 63175 Aubière, France
[b] Process Control Laboratory, ENP, Alger, Algeria

► Parallel vision/force control scheme is applied on three different mechanical structures of parallel robots with different degrees of freedom. ► Vision sensor is used to measure Cartesian poses of the robots end-effectors. ► We examine effect of the changes in the level of the sensor resolution and calibration on the position and force tracking errors. ► Tracking errors depend only on sensor performances and are not affected by the machine kinematics and dynamics complexity. Q2

UNCORRECTED PROOF

0094-114X/$ – see front matter © 2011 Published by Elsevier Ltd.
doi:10.1016/j.mechmachtheory.2011.05.010

ARTICLE IN PRESS
MAMT-01832; No of Pages 20
Mechanism and Machine Theory xxx (2011) xxx–xxx
Contents lists available at ScienceDirect
Mechanism and Machine Theory
journal homepage: www.elsevier.com/locate/mechmt

Vision/force control of parallel robots

S. Bellakehal [a,*], N. Andreff [a], Y. Mezouar [a], M. Tadjine [b]

[a] LASMEA-CNRS-Université Blaise Pascal 63175 Aubière, France
[b] Process Control Laboratory, ENP, Alger, Algeria

ARTICLE INFO

Article history:
Received 9 January 2009
received in revised form 3 May 2011
accepted 23 May 2011
Available online xxxx

Keywords:
Parallel robots
Force control
Parallel control
Visual servoing

ABSTRACT

In this paper, force and position control of parallel kinematic machines are discussed. Cartesian space computed torque control is applied to achieve force and position servoing directly in the task space within a sensor-based control architecture. The originality of the approach resides in the use of a vision system as an exteroceptive pose measurement of a parallel machine tool for force control purposes. Three different mechanical structures with different degrees of freedom are considered to validate the approach.

© 2011 Published by Elsevier Ltd.

1. Introduction

Recently, parallel robots have drawn a lot of interest in the robotic community due to their theoretical superiority over the classical serial structures in terms of stiffness, accuracy, high speed and payload in spite of their more complex kinematics and smaller workspace compared to serial manipulators. These specific benefits allowed the parallel kinematic machines to perform better some industrial tasks requiring accurate and fast motion like the pick and place of light objects. Moreover, being stiff, parallel robots have potential abilities to perform better most of machining operations (like deburring, polishing,…) than the serial ones because these lasters are subject to link deflections under external load when exerting force on a rigid environment. Such deflections have significant impact on robot performances when dealing with tasks involving both Cartesian position and contact forces control. For such tasks, the interaction force must be controlled properly, since otherwise the arising contact forces may damage the object or the robot tip. To this end, different force control approaches have been proposed in the literature and applied for serial machines. The case of parallel machines has rarely been addressed in view of the complexity of their mechanical architecture, which leads to difficulty to obtain the relation determining the pose of the end effector from the joint coordinates (Forward Kinematic Model). Indeed, solving the Forward Kinematic Model (FKM) of parallel machines remains a difficult problem. The Forward Kinematic Model is indispensable to achieve robot position control in Cartesian space (using joint sensors) which is more convenient when the interaction forces between the robot end effector and the environment must be controlled as well. Also, force control involves the dynamics of the mechanical structure which is easily described in Cartesian space for a parallel machine. An alternative to obtain the end effector Cartesian pose without calculating the fastidious Forward Kinematic Model of a parallel robot is the use of an exteroceptive measure, specially, a camera since vision systems have shown good efficiency to guide robot using image information (visual servoing). The present work focuses on coupling force feedback and visual servoing to control both contact forces and the end effector Cartesian pose of a parallel robot. The two controlled variables (contact forces and Cartesian pose of the end effector) are directly measured by exteroceptive sensors (force sensor and camera) within parallel

Q1 * Corresponding author. Tel.: +33 473407766; fax: +33 473407262.
E-mail address: Saliha.BELLAKEHAL@lasmea.univ-bpclermont.fr (S. Bellakehal).

0094-114X/$ – see front matter © 2011 Published by Elsevier Ltd.
doi:10.1016/j.mechmachtheory.2011.05.010

Please cite this article as: S. Bellakehal, et al., Vision/force control of parallel robots, Mech. Mach. Theory (2011), doi:10.1016/j.mechmachtheory.2011.05.010

UNCORRECTED PROOF

ARTICLE IN PRESS

vision/force control architecture similar to that presented in [7]. The major advantage of the proposed control scheme is the opportunity of achieving both control goals directly in the task space without any use of the manipulator's forward kinematics. Also within this control architecture, the robot dynamic non linearities are fully compensated for, position and force are explicitly controlled and both sensors (force sensor and camera) control simultaneously all directions. First, the results obtained with two different mechanical structures (with three and four DOF) are presented to show the robots inertia effects on its sensibility to the measurement noise. Then, the results obtained with a third six DOF robot are presented to show the approach efficiency for those parallel structures for which the forward kinematics is difficult to obtain.

The remainder of the paper is the following: next section presents briefly previous work on force control, parallel machines and vision/force control, Section 3 outlines the Cartesian general dynamics of the machine and the derivation of the adopted control law, Section 4 exposes the difficulties encountered in position/force control scheme of parallel robots and the proposed solution, in Section 5 a description of the three test-beds architecture is presented, the environment simulation and a discussion on the obtained results is to be found in Section 6.

2. Preliminaries

2.1. Force control

Force control is essential for tasks involving interaction between the manipulator and the environment. Different control schemes have been proposed in the literature, as surveyed by DeSchutter and Spong [14]. The two basic approaches to force control are namely hybrid position/force control [34] and impedance control [17]. On one hand, hybrid control formalism partitions the six task space degrees of freedom into purely position-controlled and purely force-controlled directions selected a priori upon an ideal description of the environment geometry. A diagonal selection matrix dictates which degrees of freedom are force-controlled and which ones are position-controlled. Two independent controllers are then independently designed for each subspace and the orthogonality of the two subspaces is ensured within this control architecture. However, the geometric description of the environment is not always perfectly known and can change at every stage of the task execution. The hybrid control formalism with a selection matrix, although applicable to many simple contact situations, has been superseded by a more general constrained-based approach in which desired motions and desired contact forces can be specified in arbitrary directions of the six-dimensional manipulation space [11]. On the other hand, impedance control aims at developing a relationship between interaction forces and end effector position in contact with the environment without controlling force explicitly. The force exerted on the environment by the manipulator is dependent on its position and its impedance, and is indirectly controlled by prespecifying a robot positional reference trajectory which is determined regarding the dynamic properties of the environment. One of the major practical difficulties with this technique is that the environment dynamic properties (stiffness, damping and inertia) are usually not known precisely so that accurate reference trajectory cannot be designed to achieve accurate contact force control. Other approaches were proposed to combine inherent advantages of both impedance and hybrid position/force control. External control [12] where the force control loop is closed around an internal position loop in a hierarchical way, and parallel (or implicit) control [7] which is able to control both position and force variables using two parallel force control and position control loops like the hybrid approach without any selection matrices. The conflict situations between the two control loop actions are managed by the dominance of the force control loop over the position control loop.

2.2. Parallel machines

Parallel structures offer superior rigidity relative to their size and weight, low mass and high acceleration with respect to existing serial machines. In the last years, they have been the subject of increasing attention and all the control schemes mentioned above which are essentially developed for serial robot manipulators, have been extended to parallel machines. Thus, hybrid control were applied to parallel mechanisms [25,36], impedance control approaches were also used [2,15,4,5] as well as external control [35,16] and parallel control [6,18]. Nevertheless, the issue of position/force control of parallel robots remains rarely addressed in the robotic literature. This is due to the additional weaknesses like the limited work volume in comparison with that of serial manipulators, and the increased computational effort necessary to their control. Such problems were widely invoked and analyzed in the literature [10,26,19,28,39]. The major problem of parallel robots is the forward kinematics consisting in finding the possible pose of the platform for given joint coordinates which is more complex than its dual inverse kinematics for serial robots. Generally, numerical approaches (e.g. Newton–Raphson) are used to solve iteratively the set of non linear Forward kinematic equations starting by an initial estimate of the solution. This method leads sometimes to a solution which does not correspond to the current pose. The analytical approach is possible only for very restrictive particular kinematic structures of parallel robots, in the general case, the analytical approach leads to solve high degree polynomial equations. These drawbacks prevent these structures from being used in many high speed real-time engineering applications in spite of their potentially higher accuracy and rigidity.

2.3. Vision/force coupling

To cope with this difficulty, a very attractive alternative to model-based control of the tool tip pose is to use an exteroceptive sensor (e.g. vision and laser) which does not make any restriction on the kinematics of the robot. Indeed, it allows to directly

Please cite this article as: S. Bellakehal, et al., Vision/force control of parallel robots, Mech. Mach. Theory (2011), doi:10.1016/j.mechmachtheory.2011.05.010

UNCORRECTED PROOF

measure the Cartesian pose of the parallel robot while traditional proprioceptive measure requires the calculation of the forward kinematic model. This idea was adopted in [30,1] using vision system for motion tracking purposes. To our knowledge, the use of cameras as position sensor in addition to the force sensor has never been suggested in the literature for the force control and motion tracking of parallel structures, whereas, it has been widely invoked in the case of serial manipulators. Indeed, the benefit of combining visual servoing and force feedback to increase the robot robustness and ability in manipulation tasks was recognized since 1973 when an insertion task was performed using visual feedback [37]. Hence, the issues concerning the integration of these two sensing modalities intrigued the robotic community: cameras are useful robotic sensors since they mimic the human sense of vision and allow the robots to locate and inspect the objects without contact. On the other hand, force sensors are useful to control the contact force in order to avoid damages in the robot end effector and manipulated object. This makes the combination of force and vision an attractive option for accurate control of contact tasks.

In [27], vision/impedance control was used for peg-in-hole insertion experiments where an image-based visual servoing controller is closed around an impedance controller. The output of the 2D visual controller is integrated to generate the reference trajectory required by the impedance controller which is limited to pure damping. The same approach is adopted in [33] with a second order impedance controller. Theories of hybrid position/force control were adopted in [29] by substituting the position control loop by position-based visual servoing which permits fast approach of the end effector toward the surface to be contacted and gives information regarding the proximity of the workpiece. In [3], an appropriate hybrid (or shared) control for eye-in-hand vision and force integration was proposed, placed into a global 3D framework based on Mason's task frame formalism. In this work, a simulated 3D visual servoing loop is achieving motion control while a force control loop regulates contact forces via force feedback. This requires the derivative of the robot dynamic model.

3. General dynamics and control

Computed torque control is widespread for serial manipulators. It can be applied ever in joint space or in Cartesian space. However, joint space control is incompatible with the requirements of constrained tasks, which involve simultaneous motion and force control [22]. So, force control algorithms must take into account dynamic interaction between the end-effector and the manipulated object at the task space level to achieve higher performances. For parallel robots, the Cartesian space computed torque control was shown more suitable [10] since the natural description of parallel machine dynamics is in the task space, in addition, the variables to be controlled are naturally defined in the task space. This nonlinear Cartesian dynamic decoupling approach was adopted in [6] within the parallel position/force control architecture introduced by Chiaverini [7] for a position/force controlled parallel robot as depicted in Fig. 1.

Defining x as a set of independent Cartesian generalized coordinates, if the manipulator is interacting with the environment and exerting a force F in the task space, the equation of motion can be written as:

$$A_x(x)\ddot{x} + C_x(x,\dot{x}) + G_x(x) + F + D^t_{inv}(x)\Gamma_f = \Gamma_x \tag{1}$$

with:

$$x = FKM(q), q = IKM(x) \tag{2}$$

$$\begin{aligned}\dot{x} &= D^{-1}_{inv}(x)\dot{q}, \dot{q} = D_{inv}(x)\dot{x} \\ \ddot{x} &= D^{-1}_{inv}(x)\ddot{q} + \dot{D}^{-1}_{inv}(x)\dot{q},\end{aligned} \tag{3}$$

$$\ddot{q} = D_{inv}(x)\left[\ddot{x} - \dot{D}^{-1}_{inv}(x)\dot{q}\right] \tag{4}$$

$$\Gamma_x = D^t_{inv}(x)\Gamma, \Gamma = D^{-t}_{inv}(x)\Gamma_x \tag{5}$$

where q is the generalized coordinate vector, $A_x(x)$ is the symmetric and positive definite Cartesian space inertia matrix, $C_x(x,\dot{x})$ is the vector representing Coriolis and centrifugal terms in the Cartesian space, $G_x(x)$ is the vector of Cartesian gravitational terms, Γ_f represents the vector of friction forces, Γ is the vector of generalized torques at the joints and Γ_x its projection in the task frame, $D_{inv}(x)$ is the inverse instantaneous kinematic matrix also known as the inverse kinematic Jacobian matrix of the robot. Notice that for a general parallel machine, the forward instantaneous kinematic matrix $D^{-1}_{inv}(x)$ is obtained by inverting numerically the inverse instantaneous kinematic matrix $D_{inv}(x)$ (which is easier to obtain for most parallel structures) since the forward kinematic model is not available analytically.

Under the hypothesis that the system model is perfectly known, the non linear dynamic decoupling approach [21] is thus applied to the motion Eq. (1) which leads to the following control law:

$$\Gamma_x = \hat{A}_x(x)u + \hat{C}_x(x,\dot{x}) + \hat{G}_x(x) + \hat{F} + D^t_{inv}(x)\hat{\Gamma}_f \tag{6}$$

UNCORRECTED PROOF

Please cite this article as: S. Bellakehal, et al., Vision/force control of parallel robots, Mech. Mach. Theory (2011), doi:10.1016/j.mechmachtheory.2011.05.010

ARTICLE IN PRESS

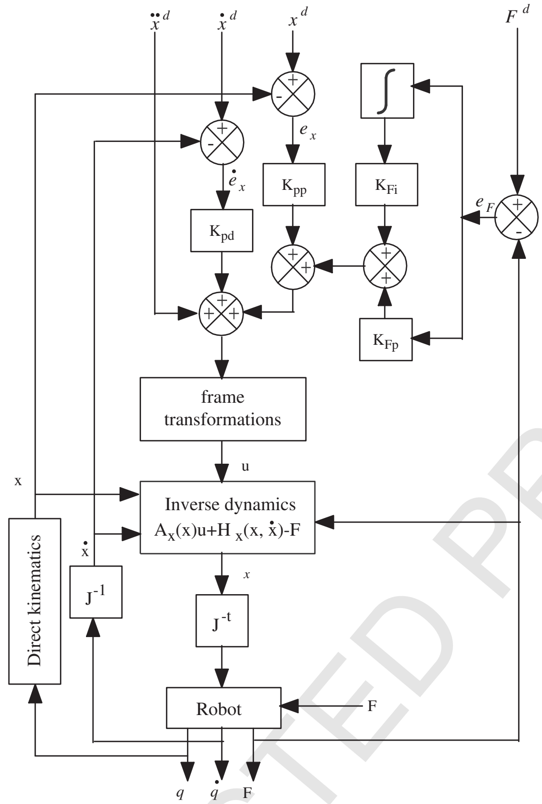

Fig. 1. The parallel force position control scheme adopted in [6].

where $\hat{A}_x$, $\hat{C}_x$, $\hat{G}_x$, $\hat{F}$ and $\hat{\Gamma}_f$ are estimated values of A_x, C_x, G_x, F and Γ_f respectively. By choosing the auxiliary input control u as the Cartesian acceleration, a linearization by non linear feedback is hence possible. Assuming that position and force control loops are respectively a linear PD and PI control laws (see Fig. 1):

$$u_p = \ddot{x}^d + K_v\left(\dot{x}^d - \dot{x}\right) + K_p\left(x^d - x\right) \tag{7}$$

$$u_f = K_f\left(F^d - F\right) + K_i\int_0^t\left(F^d - F\right)d\tau \tag{8}$$

with:

$$u = u_p + u_f \tag{9}$$

where x^d, $\dot{x}^d$ and F^d are respectively the desired values of the Cartesian position, its derivative and the contact forces. The resultant control law applied to the actuators can hence be written as:

$$\Gamma_x = \hat{A}_x(x)\left[\ddot{x}^d + K_v\left(\dot{x}^d - x\right) + K_p\left(x^d - x\right) + K_f\left(F^d - F\right) + K_i\int_0^t\left(F^d - F\right)d\tau\right] + \hat{C}_x(x,\dot{x}) + \hat{G}_x(x) + \hat{F} + D_{inv}^t(x)\hat{\Gamma}_f. \tag{10}$$

This control law allows for explicit servoing of both position and force variables along all directions of the task space with dominance of force control loop over the position one thanks to the integral action.

4. Vision/force control

In the control scheme depicted in Fig. 1, the calculation of the forward kinematics of the parallel robot is required to achieve Cartesian position control. As mentioned above, the analytical equations of the forward kinematic model are not available for any parallel robot and the numerical methods can fail to reach the actual pose (convergence difficulty). To deal with these troubles, the idea we are proposing is to replace the forward kinematic model by an exteroceptive sensor which gives directly the measured value of the platform pose instead of solving a set of non linear equations. Indeed, in the control scheme presented in Fig. 1, a

Please cite this article as: S. Bellakehal, et al., Vision/force control of parallel robots, Mech. Mach. Theory (2011), doi:10.1016/j.mechmachtheory.2011.05.010

UNCORRECTED PROOF

ARTICLE IN PRESS

sensor-based force control loop is coupled with a model-based position control loop which is not homogeneous in terms of control architecture. Furthermore, the presence of a numerically estimated model in the control loop can lead to a lack of stability, reliability and accuracy, while increasing the computational cost. Note also that a model-based control is inherently less robust with respect to modeling errors.

On the opposite, using an exteroceptive measure, one has only to deal with one potential source of errors (Cartesian pose measurement errors) which is directly sent to the controller. In this case, all uncertainties due to geometric errors and joint backlashes do not affect the control loop. Furthermore, one can decrease the computational cost since no calculation of forward kinematic model is needed. In addition, contrary to the control scheme presented in Fig. 1, motion and force are addressed at the same control level. As a result, pose and contact forces are controlled in the task frame within a homogeneous sensor-based control approach. In conclusion, there is a clear need for the end effector pose measurement in the task space to deal with the requirements of constrained tasks and high speed applications. To this end, some measuring devices can be employed:

Wire based systems: A number of wires are connected to the robot end effector to constitute tetrahedra and the pose is estimated by mean of trilateration (reconstruction of the pose from the length of tetrahedra edges) as in the CaTraSys system [40]. This technique has low cost but is not completely safe since wires can constitute a physical limitation (interference among wires and wrapping risks). In addition, wires can be seen as extensible legs, so this problem is equivalent to that of solving the kinematics of a parallel manipulator. Thus, using this device means that one is replacing the problem of solving the kinematics of a parallel machine by solving the same problem.

Mechanical device: One could also add a serial mechanism in parallel with the parallel robot and calculate its pose (e.g. Faro or Romer arms), which is the same as the parallel robot's one, by means of the well known Forward Kinematics of serial structures. The added measuring mechanism can even have a parallel architecture like Gough–Stewart platform [8]. This method is limitative since the added robot must be sufficiently light to limit the influence on the parallel robot dynamics and thus it may be subject to flexion leading to non accurate pose estimation. Also with this technique, one cannot obtain redundancy in the measured information since we have just six measures to determine the six Cartesian pose variables.

Laser interferometer: This device can precisely guide the robot at high sampling rate if appropriately calibrated but it is expensive and very restrictive regarding its sensitivity to environmental effects (namely, the laser beam must not be interrupted). Also when possible, the orientation measurement is not very accurate.

Vision system: A vision system needs calibration but it is suitable for a large class of structures and does not make any assumption on the kinematics of the robot. It is low cost, safe, easy to use (without any physical interaction) and rather accurate since it allows easily to obtain redundant information on the end effector pose.

In view of the growing efficiency of image processing algorithms and image acquisition technology, vision constitutes an adequate sensor that we propose to employ for end effector pose measurement. In this way, the force/position control scheme proposed in [6] (Fig. 1) can be reduced to the one depicted in Fig. 2 where no calculation of the Forward Kinematic Model is required. In this control scheme, both force and position variables are controlled in the task space by means of two control loops acting in parallel. As mentioned in Section 1, and regarding the complementarity between the force and vision sensors, coupling vision and force is indeed more than convenient in the case of parallel robots since it additionally avoids the Forward Kinematic problem and allows to compensate for the kinematic errors.

Notice that even the end effector velocity measurement can be available from vision according to [1]. A more recent work developed in our laboratory [9] uses a strategy based on an acquisition of selected regions of interest which decreases the density of the transmitted data. An estimation frequency of 333 Hz was reached experimentally with a fairly good accuracy. Therefore, no numerical differentiation may appear in the motion control loop.

5. Modeling of the test-beds

The proposed approach illustrated in Fig. 2 will be applied on three different mechanical structures: a heavy four DOF (degrees of freedom) parallel robot, the Isoglide-4 T3R1, a light one, the Orthoglide (three DOF), and a six DOF robot, the DeltaLab which is a Gough–Stewart type machine. Kinematic and dynamic modeling which are required to achieve control purposes have to be recalled in the next subsections for each parallel robot for the sake of completeness.

5.1. The Orthoglide

5.1.1. Presentation

The Orthoglide is a Delta-type PKM dedicated to 3-axis rapid machining applications that was designed at IRCCyN [23]. Its mechanical structure is constituted of three identical legs (Fig. 3) which are PRPaR chains (P: Prismatic, R: Revolute, Pa: Parallelogram) with only one actuated joint (the prismatic one), this leads to a pure translational motion of the tool like conventional PPP machines (Fig. 3). The model used in this study is the light weight structure prototype which was originally developed at IRCCyN in 2000–2001 to validate the kinematic architecture [41]. Its maximal performances are $1.2m.s^{-1}$ for speed and $20m.s^{-2}$ for acceleration (much more faster compared to the Isoglide-4 T3R1).

Please cite this article as: S. Bellakehal, et al., Vision/force control of parallel robots, Mech. Mach. Theory (2011), doi:10.1016/j.mechmachtheory.2011.05.010

ARTICLE IN PRESS

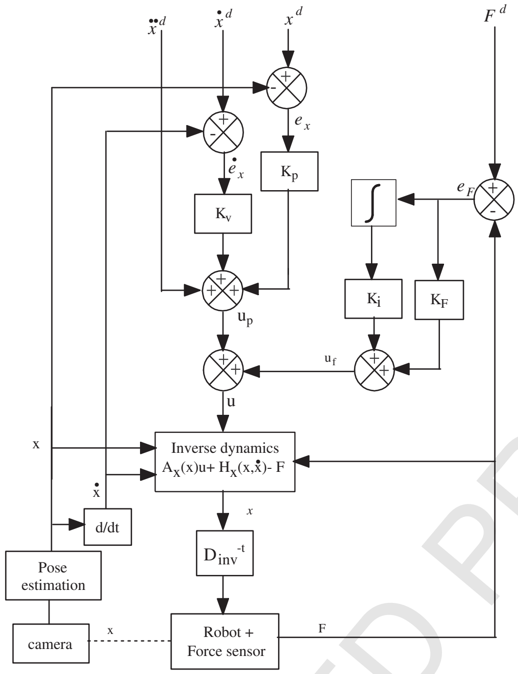

Fig. 2. The proposed parallel vision/force control.

5.1.2. Kinematic modeling

The Orthoglide has the advantage of having an analytically defined forward kinematic model linking the active joint variables (q_i, $i = 1, 2, 3$) to the end-effector Cartesian coordinates (x_e, y_e, z_e) through second order equations whose solution is [32]:

$$\begin{cases} x_e = P_2 + t/P_2 \\ y_e = P_3 + t/P3 \\ z_e = P_1 + t/P_1 \end{cases} \tag{11}$$

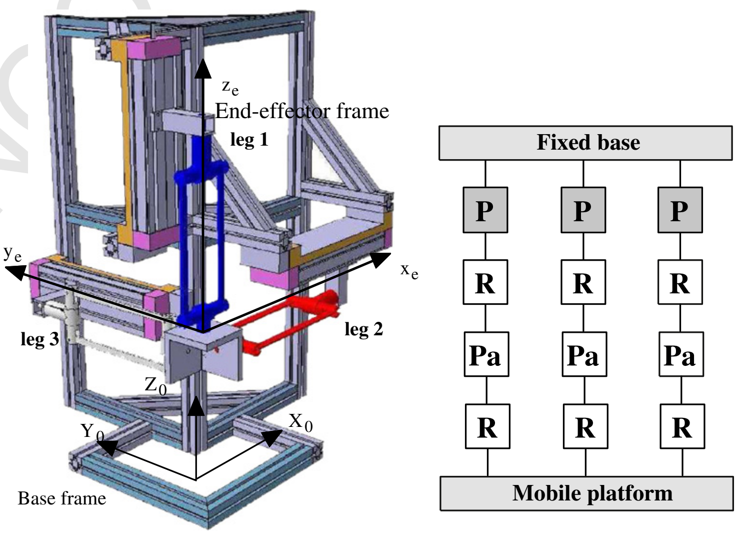

Fig. 3. Global view of the Orhtoglide (left) and its kinematic scheme (right).

UNCORRECTED PROOF

Please cite this article as: S. Bellakehal, et al., Vision/force control of parallel robots, Mech. Mach. Theory (2011), doi:10.1016/j.mechmachtheory.2011.05.010

ARTICLE IN PRESS

where:

- $P_i = \frac{1}{2}(-d + q_i)$ for $i = 1, 2, 3$
- $t = \frac{-B \pm \sqrt{B^2 - 4AC}}{8A}$

with:

$$A = \frac{1}{16}\sum_{i=3}^{3} P_i^{-2}, \quad B = \frac{1}{2}, \quad C = \left(\sum_{i=3}^{3} P_i^2\right) - L^2$$

where d is the origin of each axis and L is the length of the parallelogram. The inverse instantaneous kinematic model linking joint speeds to the end-effector velocity is then given by:

$$D_{inv}(x) = \begin{pmatrix} \frac{x_e}{\Delta_1} & \frac{y_e}{\Delta_1} & 1 \\ 1 & \frac{y_e}{\Delta_2} & \frac{z_e - a}{\Delta_2} \\ \frac{x_e}{\Delta_3} & 1 & \frac{z_e - a}{\Delta_3} \end{pmatrix} \tag{12}$$

where:

$$\Delta_1 = \sqrt{L^2 - x_e^2 - y_e^2}$$
$$\Delta_2 = \sqrt{L^2 - y_e^2 - (z_e - a)^2}$$
$$\Delta_3 = \sqrt{L^2 - x_e^2 - (z_e - a)^2}$$

5.2. The Isoglide-4 T3R1

5.2.1. Presentation

The mechanical structure of the fully isotropic parallel machine the Isoglide4-T3R1 has four DOF with three translations and one rotation θ (Fig. 4) around Y axis. It is constituted of a fixed base connected to the payload platform by means of four identical legs (two horizontal and two vertical) which are PRRU chains, each leg contains three links: the first one is connected to the fixed base and is actuated with a prismatic joint (linear actuator); the second one has its two extremities connected to the first and the third ones with two passive revolute joints (fixed length); the mobile platform is connected to the third leg by a universal joint (fixed length) as presented in Fig. 4. This machine is designed for high speed machining and can reach $10 m.s^{-1}$ while its maximal acceleration is limited at $3 m.s^{-2}$ due to its inertia. In fact, the structure weight is important to satisfy the stiffness requirements: 31 kg for each leg and 14 kg for the mobile platform.

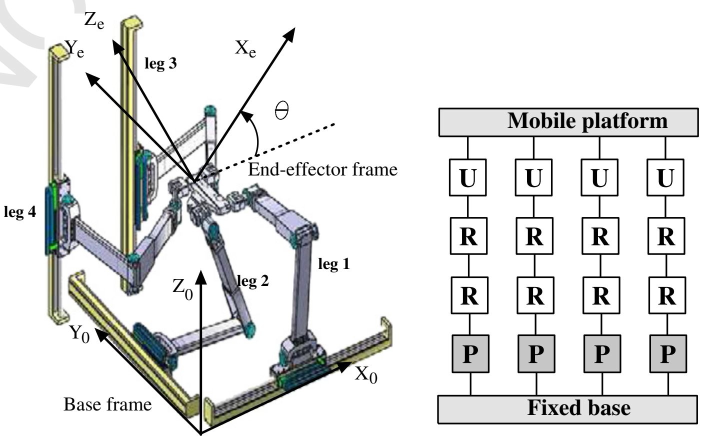

Fig. 4. Structure of the Isoglide4-T3R1 (left) and its kinematic scheme (right).

UNCORRECTED PROOF

Please cite this article as: S. Bellakehal, et al., Vision/force control of parallel robots, Mech. Mach. Theory (2011), doi:10.1016/j.mechmachtheory.2011.05.010

ARTICLE IN PRESS

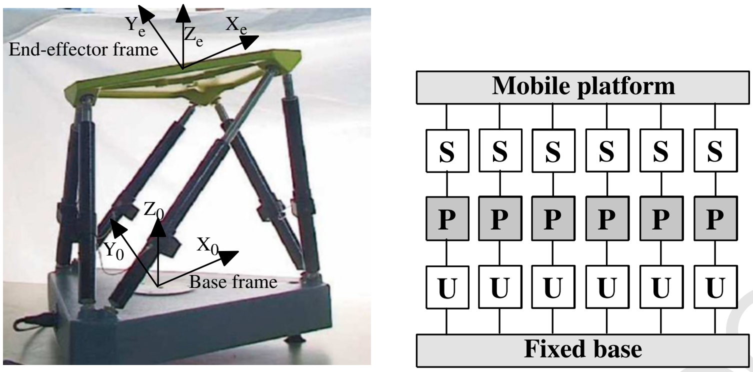

Fig. 5. A pedagogic implementation of the Gough–Stewart platform (left) and its kinematic scheme (right).

5.2.2. Kinematic modeling

The main advantage of the Isoglide-4 T3R1 is to have an almost decoupled structure leading to a simple expression of the forward kinematics giving the Cartesian end-effector pose (x_e, y_e, z_e, θ) as a function of active joint variables:

$$\begin{cases} x_e = q_1 - x_0 \\ y_e = q_2 - y_0 \\ z_e = q_3 - z_0 \\ \sin\theta = \dfrac{q_4 - q_3 + \delta z}{L} \end{cases} \tag{13}$$

where L is the characteristic length of the moving platform (i.e. the distance between the attachment points of legs 3 and 4 onto the platform) and δz is the distance along the z_0 axis between the origins of joints 3 and 4. The inverse instantaneous kinematics model is derived from the inverse kinematics in a straightforward way, the expression obtained close to the identity matrix:

$$D_{inv}(x) = \begin{pmatrix} 1 & 0 & 0 & 0 \\ 0 & 1 & 0 & 0 \\ 0 & 0 & 1 & 0 \\ 0 & 0 & 1 & L\cos\theta \end{pmatrix} \tag{14}$$

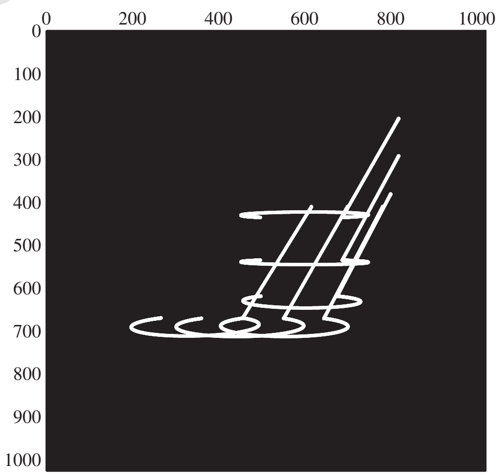

Fig. 6. Projection of the Orthoglide desired trajectory in the image plane using a 6 blob visual pattern.

Please cite this article as: S. Bellakehal, et al., Vision/force control of parallel robots, Mech. Mach. Theory (2011), doi:10.1016/j.mechmachtheory.2011.05.010

UNCORRECTED PROOF

ARTICLE IN PRESS

Table 1
Desired trajectory of the Orthoglide.

	x_e (m)	y_e (m)	z_e (m)
x_0	0.00	0.00	0.34
x_c	0.1	−0.1	0.24
Δx	0.1	−0.1	−0.1

5.3. The Gough–Stewart robot

5.3.1. Presentation

As a last example, we consider the Gough–Stewart platform as representing a generic robot with full position and orientation capabilities. This robot is a 6-UPS (Universal-prismatic-spherical) structure constituted of two bodies connected with six extendable legs which are actuated with prismatic joints. Each leg is connected trough spherical joint at the mobile platform and through universal joint at the fixed base. The implementation we have is the DeltaLab robot which was designed for academic and teaching purposes. This mechanism has two triangular bodies: a fixed base of radius 270 mm and a mobile platform of radius 195 mm (Fig. 5).

5.3.2. Kinematic modeling

Like the most of hexapods, the forward kinematic of the Gough–Stewart robot is difficult to be solved and no analytic formulation is available, whereas, its inverse kinematic model have the simpler form:

$$q_i^2 = \overrightarrow{A_iB_i}^t \, \overrightarrow{A_iB_i} \quad \forall i \in 1..6 \tag{15}$$

where A_i are the points of attachment between the legs and the base and B_i are the points of attachment between the legs and the mobile platform. This model express that q_i is the length of vector $\overrightarrow{A_iB_i}$.

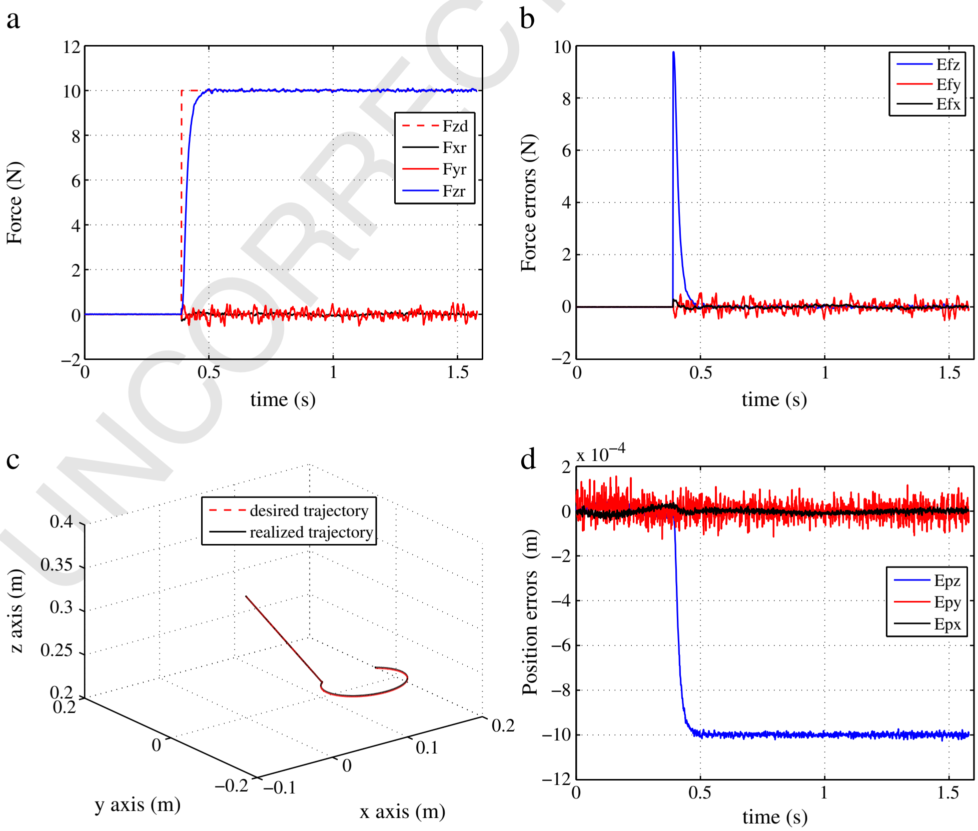

Fig. 7. Results obtained with the Orthoglide in Case 1: (a) Desired and realized forces, (b) force errors, (c) 3D Cartesian trajectory, (d) Cartesian position errors.

Please cite this article as: S. Bellakehal, et al., Vision/force control of parallel robots, Mech. Mach. Theory (2011), doi:10.1016/j.mechmachtheory.2011.05.010

UNCORRECTED PROOF

5.4. Dynamic modeling

A general solution for the dynamic modeling of parallel kinematic machines was proposed in [20]. In most cases, this method should lead to an inverse dynamic model which depends only on Cartesian space variables. This property is suitable for Cartesian space computed torque control. According to Khalil's formulation which is adopted here, the dynamics of the mobile platform is calculated as a function of the Cartesian variables ($x, \dot{x}$ and $\ddot{x}$), whereas the dynamics of the legs are calculated as a function of the joint variables of the legs ($q, \dot{q}$ and $\ddot{q}$). As a result, the dynamics of the overall parallel structure can be presented as [20]:

$$\Gamma = D_{inv}^{-t}(x)\left[F_p + \sum_{i=1}^{k} J_{pi}^t J_i^t H_i\right] + \Gamma_f \tag{16}$$

where F_p is the dynamics of the mobile platform, k is the legs number, J_{pi} a Jacobian matrix linking the Cartesian coordinates of the end of the leg i to the Cartesian coordinates of the end effector, J_i the Jacobian matrix of the serial kinematic structure of the leg i, Γ_f is the friction forces term and H_i is the inverse dynamic model of the leg i seen as a single serial machine. Many well known methods can be used to calculate H_i as a function of passive and active joints of the leg i. However, in most cases, parallel robots have quite simple legs with few joints (three or four). Thus, linking passive joint variables to the end-effector pose is easy with trivial trigonometry, whereas, the active joint variables are linked to the end-effector pose with the algebraic inverse kinematic model depending on the end-effector pose. Consequently, each term depends algebraically on the end-effector pose as mentioned above. The friction forces term Γ_f is composed of viscous and dry friction forces Γ_{fv} and Γ_{fs} respectively:

$$\Gamma_f = \Gamma_{fv} + \Gamma_{fs} = F_v\dot{q} + F_s sign(\dot{q}) \tag{17}$$

UNCORRECTED PROOF

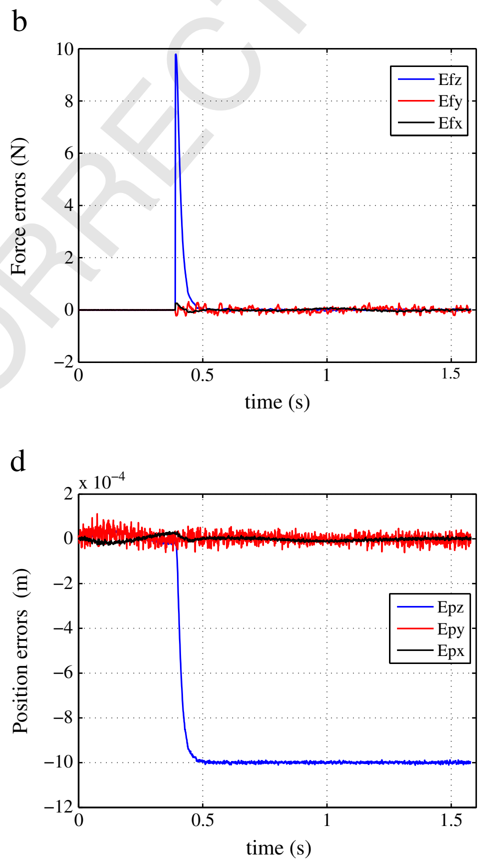

Fig. 8. Results obtained with the Orthoglide in Case 2: (b) force errors, (d) Cartesian position errors.

Please cite this article as: S. Bellakehal, et al., Vision/force control of parallel robots, Mech. Mach. Theory (2011), doi:10.1016/j.mechmachtheory.2011.05.010

where F_v and F_s are viscous and dry friction parameters. Newton–Euler formalism is used to derive the dynamics of the mobile platform. Assuming that the end effector is exerting a force F on the environment, the dynamics of the mobile platform is given in the general case of six DOF by the following Newton–Euler equation:

$$F_p = A_p\ddot{x} + \begin{bmatrix} \Omega \times \left(\Omega \times MS_p\right) \\ \Omega \times \left(I_p\Omega\right) \end{bmatrix} - \begin{bmatrix} m_pI_3 \\ M\tilde{S}_p \end{bmatrix} g + F \tag{18}$$

where:

- A_p: is the 6×6 spatial inertia matrix of the platform given by:

$$A_p = \begin{bmatrix} m_pI_3 & -M\tilde{S}_p \\ M\tilde{S}_p & I_p \end{bmatrix}$$

- I_p is the (3×3) inertia matrix of the platform.
- Ω: is the angular velocity of the platform.
- $M\,S_p$: is the 3×1 vector of first moments of the platform around the origin of the platform frame,

$$M\,S_p = \left[M\,X_p \quad M\,Y_p \quad M\,Z_p\right]$$

- $M\tilde{S}_p$: designates the (3×3) skew matrix associated with the vector.
- m_p: is the masse of the platform.

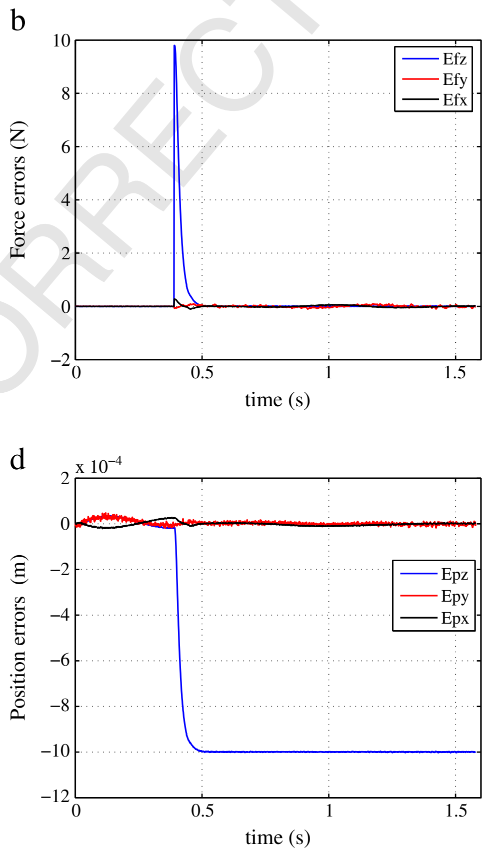

Fig. 9. Results obtained with the Orthoglide in Case 3: (b) force errors, (d) Cartesian position errors.

UNCORRECTED PROOF

Please cite this article as: S. Bellakehal, et al., Vision/force control of parallel robots, Mech. Mach. Theory (2011), doi:10.1016/j.mechmachtheory.2011.05.010

ARTICLE IN PRESS

- I_3: is the 3×3 identity matrix.
- g: is the acceleration of gravity.
- F: is the force exerted on the environment.

Only the terms along the end-effector degrees of freedom are retained. Thus, in the case of the Orthoglide and all translational robot, bias forces (or coriolis and centrifugal terms) resulting from the angular velocity of the mobile platform are not considered. The Orthoglide end-effector dynamics is then reduced to:

$$F_p = m_p(\ddot{x} - g) + F. \tag{19}$$

Detailed expressions of the Orthoglide dynamic model can be found in [31] where an experimentally validation of this model was conducted. In the Isoglide-4 T3R1 case, the inverse dynamic model is more complex since a fourth DOF is added, but it still has a closed-form expression depending on the end-effector pose. Detailed expression and experimental validation of the Isoglide-4 T3R1 dynamic model can be found in [30]. The Gough–Stewart platform is considered as representing the common problems of parallel robots dynamics and an explicit method to calculate the dynamic model of a general Gough–Stewart platform can be found in [17] or [10].

Notice that in [20], the contact force F between the end-effector and the environment is not considered and the effector is assumed to move in free space only. However, constrained motion is addressed in this work and the surface with which the effector interacts is modeled as a spring with a constant stiffness matrix K_e. The contact model is expressed as:

$$F = K_e \Delta x \tag{20}$$

where Δx is the deviation of the effector from the nominal position. In the next section, these kinematic and dynamic models are used to simulate the behavior of the three parallel robots under the parallel force/visual control scheme presented above.

UNCORRECTED PROOF

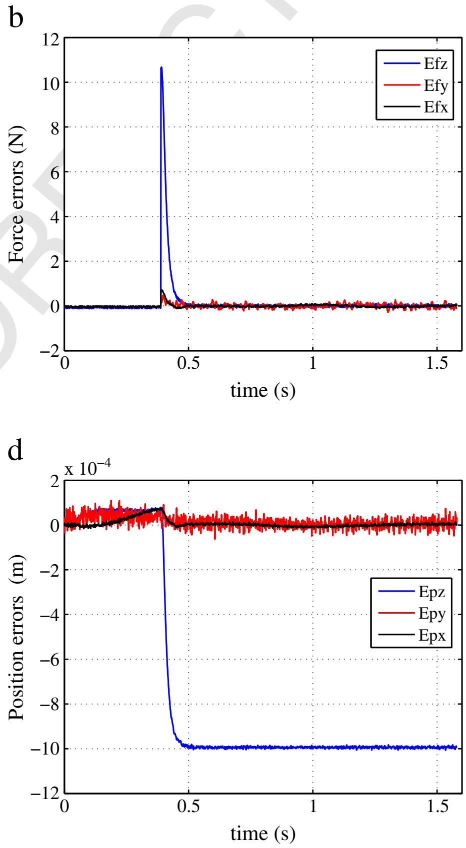

Fig. 10. Results obtained with the Orthoglide in Case 4: (b) force errors, (d) Cartesian position errors.

Please cite this article as: S. Bellakehal, et al., Vision/force control of parallel robots, Mech. Mach. Theory (2011), doi:10.1016/j.mechmachtheory.2011.05.010

ARTICLE IN PRESS

6. Simulation

6.1. Simulation environment

The dynamic models of the Orthoglide, the Isoglide4-T3R1 and the Gough–Stewart hexapod were implemented within a Matlab/Simulink environment using the dynamic and kinematic models explained in the previous section. In all this simulation, an uncertainty of 10% is added to the identified dynamic model parameters and $50\mu m$ on the geometric parameters is considered. Under the assumption that the tool axis is rigidly fixed at the center of the mobile platform and that the contact surface is parallel with the x–y plane, the contact model is assumed to have a linear force/displacement dependence via the stiffness matrix as is expressed in Eq. (20) where the stiffness value coefficient of the contact surface is set as:

$$k_e = 10^4 N.m^{-1}$$

The resolution of the adopted force sensor (Gamma sensor of ATI) is equal to $\left[\frac{1}{160}N, \frac{1}{160}N, \frac{1}{80}N, \frac{1}{32000}N.m, \frac{1}{32000}N.m, \frac{1}{32000}N.m\right]$.

6.2. Vision system and pose estimation

The vision system is modeled as a virtual perspective camera (pinhole model) in an eye-to-hand configuration. Namely, the camera observes the pose of the mobile platform with respect to the manipulator base. Hence the camera can easily be encapsulated between the legs, safely from the environment. The camera is assumed to be calibrated (with a 1024×1024 resolution and a 1.2 pixel/mm focal length) and distortion is assumed to be compensated for. The projection of a metric point in

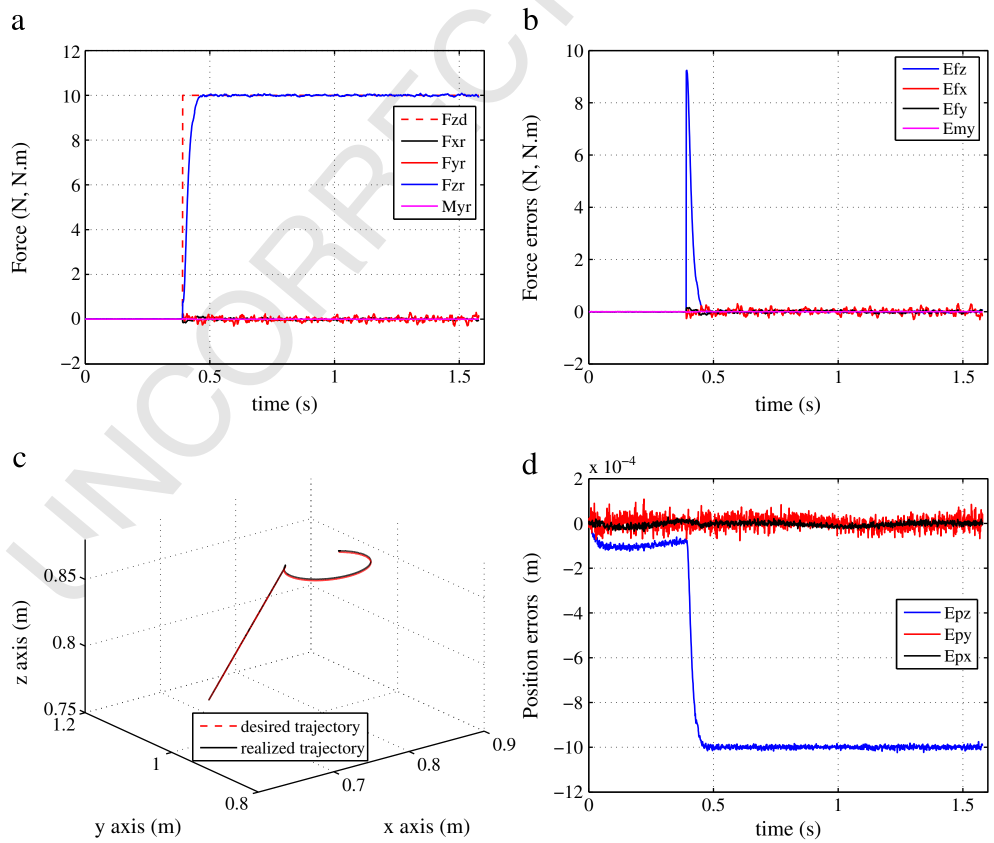

Fig. 11. Results obtained with the Isoglide in Case 1: (a) Desired and realized forces, (b) force errors, (c) 3D Cartesian trajectory, (d) Cartesian position errors.

Please cite this article as: S. Bellakehal, et al., Vision/force control of parallel robots, Mech. Mach. Theory (2011), doi:10.1016/j.mechmachtheory.2011.05.010

ARTICLE IN PRESS

the observed object frame $P=[X\ Y\ Z\ 1]^t$ into pixelic point $m=[u\ v\ 1]^t$ expressed in the image frame is given by the well-known relation:

$$m = K\left[I_{3\times3} \quad 0_{3\times1}\right]\begin{bmatrix} {}^{camera}R_{objet} & {}^{camera}t_{objet} \\ 0 & 1 \end{bmatrix}\begin{bmatrix} X \\ Y \\ Z \\ 1 \end{bmatrix} \tag{21}$$

were K is a matrix containing the intrinsic camera parameters.

The pose estimation of an object is possible with a unique camera if its 3D model and the camera parameters are known. In our simulations, the observed object is a pattern composed of 16 blobs (only 6 blobs were used in the simulation as depicted in Fig. 6). Its 3D model was precisely determined off line. The pose estimation is achieved via virtual visual servoing method which defines the pose computation problem as 2D visual servoing. This method minimizes the errors between the features extracted from the real image and the same features computed by perspective projection. The convergence of this optimization problem is ensured if the error is small enough [24]. This condition is largely verified in our application since the images of two successive 3D poses are nearby. Only the first initial image has to be sufficiently well approximated. For this purpose, the well-known Dementhon algorithm [13] is used in the first iteration. Several levels of calibration errors are simulated by a random disturbance applied once on the intrinsic parameters of the camera. A uniform noise is also added at each image to simulate measurement noises (Table 1):

Case 1: A low cost vision system with a roughly calibrated camera is used and precision of 0.1 pixel is considered. The resolution of the force sensor given above is kept.

Case 2: A highly sophisticated vision system with precisely calibrated camera is used and a precision of 0.05 pixel is considered. This precision is realistic and currently available [9]. The same resolution is kept for the force sensor.

Case 3: A futuristic case is considered and a precision of 0.01 pixel is taken. This precision is available now only in the static case not at high frame rates. The same resolution force sensor is kept.

Case 4: A fourth and last case is considered in which the accuracy of the force sensor is ten times less than the previous three cases with the vision system used in Case 2.

UNCORRECTED PROOF

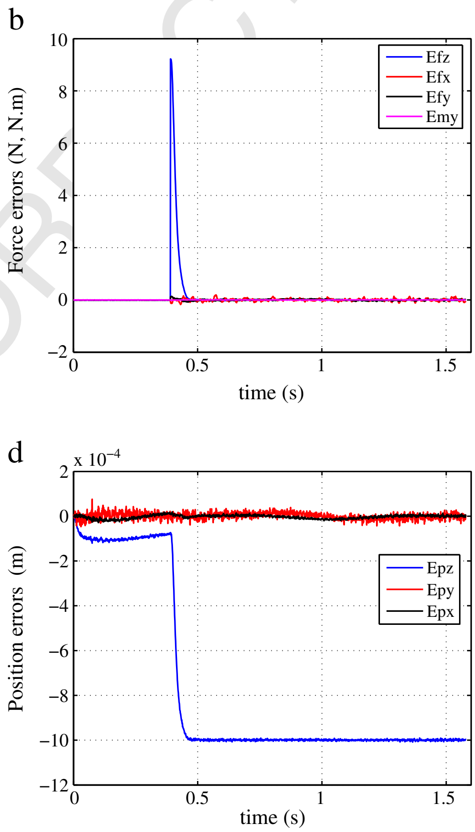

Fig. 12. Results obtained with the Isoglide in Case 2: (b) force errors, (d) Cartesian position errors.

Please cite this article as: S. Bellakehal, et al., Vision/force control of parallel robots, Mech. Mach. Theory (2011), doi:10.1016/j.mechmachtheory.2011.05.010

ARTICLE IN PRESS

7. Results

In Figs. 7 to 14, the following subfigures are given: subfigure (a) displays both the desired and actual contact forces/moments; subfigure (b) displays the difference between the desired and actual contact forces/moments; subfigure (c) shows both the desired and actual 3D trajectories of the tool; and subfigure (d) displays the difference between the desired and actual tool position coordinates along the trajectory. The tool of each robot is initially not in contact with the work surface at the initial position x_0. It has to exert a constant force of 10 N perpendicularly to the contact surface (along the z-axis direction) while following a circular trajectory of 0.05m diameter.

The Orthoglide tool is initially at $x_0=[0.0; 0.0; 0.34]^t$ expressed in its base frame and has to track a circular trajectory on a surface fixed at 0.24m from the base along the Z axis around $x_c=x_0+[0.1;-0.1;-0.1]^t$ as resumed in Table 2. The corresponding image trajectory is shown in Fig. 6 with an object composed of only six blobs to have a compromise between computational time and accuracy. Note that in [9], an object composed of sixteen blobs is used and a pose computation at 400 Hz is realized.

The Isoglide tool is initially at $x_0=[0.676, 1.047; 0.771; 0.112]^t$ expressed in its base frame and it has to track a circular trajectory on a surface fixed at 0.871 m from the base along the Z axis around $x_c=x_0+[0.1, -0.1, 0.1, 0.0]^t$ as resumed in Table 2.

To obtain the same temporal and spatial trajectories, the same performances are imposed to the two robots. Thus, the lowest maximum speed (1.2 $m.s^{-1}$) and the lowest maximum acceleration (3 $m.s^{-2}$) are taken to generate the reference trajectory using a fifth order polynomial time interpolation.

A different reference trajectory including orientation variations is imposed to the Gough–Stewart platform since this robot is taken specially to show the approach efficiency for spatial architectures with full orientation capabilities. The Gough–Stewart robot tool is initially at $x_0=[0.1, 0.1; 0.4; 0.4; 0.4; 0.4]^t$ expressed in its base frame (the orientation is represented with a ZYZ parametrization of Euler angles). It has to come into contact with a surface fixed at 0.46m from the base along the Z axis and to track two linear trajectories with orientation around Z axis (as summarized in Table 3) while exerting a perpendicular force onto the surface. The same six blobs object of Fig. 6 is used with the Isoglide4-T3R1 and the Gough–Stewart hexapod, the corresponding image trajectory figures were omitted here to avoid repetition.

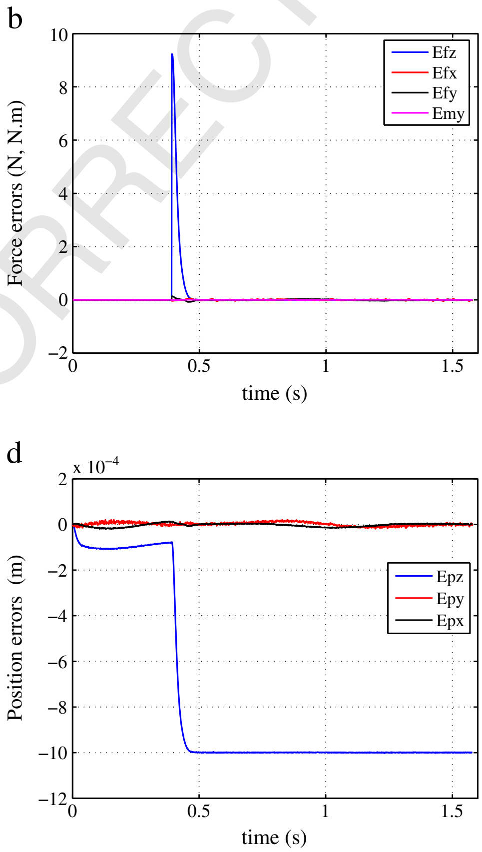

Fig. 13. Results obtained with the Isoglide in Case 3: (b) force errors, (d) Cartesian position errors.

Please cite this article as: S. Bellakehal, et al., Vision/force control of parallel robots, Mech. Mach. Theory (2011), doi:10.1016/j.mechmachtheory.2011.05.010

UNCORRECTED PROOF

ARTICLE IN PRESS

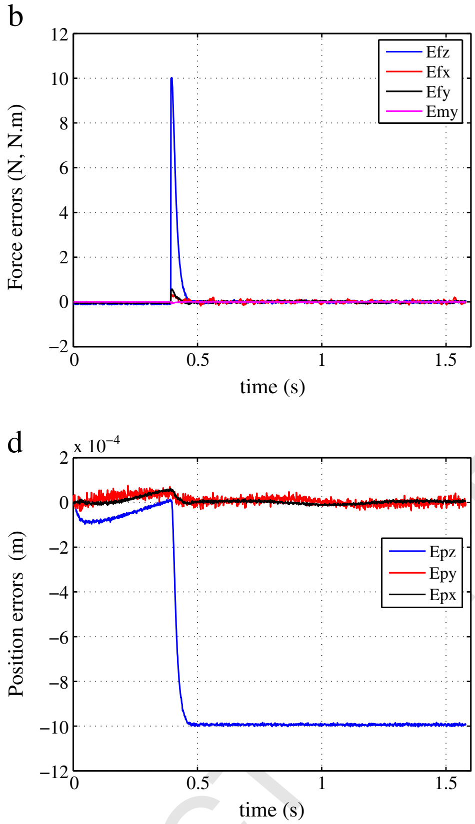

Fig. 14. Results obtained with the Isoglide in Case 4: (b) force errors, (d) Cartesian position errors.

In all cases and for the three robots, the constant gains of the controller in Eq. (10) are the same. It has been shown [38] that, along such direction, the system is stable if the gains k_p, k_v, k_f and k_i (which are tuned using Ziegler–Nichols method) satisfy the following condition:

$$k_i < k_v\left(\frac{k_p}{\hat{k}_e} + k_f\right) \tag{22}$$

where $\hat{k}_e$ is an estimate of contact surface stiffness. The following values have been chosen in the simulations: $k_p = 3(2\pi\omega)^2$, $k_v = 3(2\pi\omega)$, $k_f = 0.05\omega$ and $k_i = 5\omega$ where ω is tuned at 10 rad/s under *1KHz* sampling rate. With those values, Eq. (22) becomes $\hat{k}_e < 4.10^4 N.m^{-1}$ which does not constrain the choice of $\hat{k}_e$ in practice.

Table 2
Desired trajectory of the Isoglide-4 T3R1.

	x_e (m)	y_e (m)	z_e (m)	$\theta(rad)$
x_0	0.676	1.049	0.771	0.112
x_c	0.776	0.949	0.871	0.112
Δx	0.1	−0.1	0.1	0.0

Table 3
Desired trajectory of the Gough–Stewart robot.

	x_e (m)	y_e (m)	z_e (m)	$\alpha(rad)$	$\beta(rd)$	$\gamma(rd)$
x_0	0.1	0.1	0.4	0.4	0.4	0.4
Δx_1	−0.05	0.0	0.06	−0.3	−0.3	−0.3
Δx_2	−0.05	−0.05	0.0	0.0	0.0	0.3
Δx_3	0.05	−0.05	0.0	0.0	0.0	−0.3

Please cite this article as: S. Bellakehal, et al., Vision/force control of parallel robots, Mech. Mach. Theory (2011), doi:10.1016/j.mechmachtheory.2011.05.010

ARTICLE IN PRESS

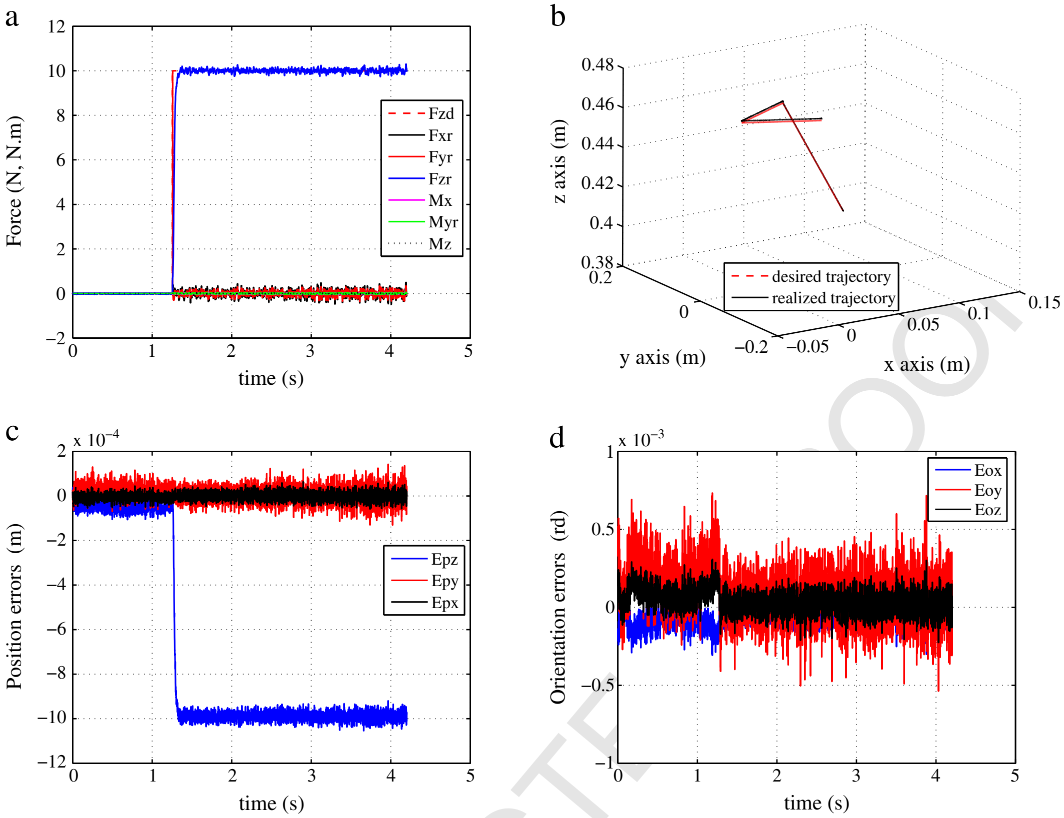

Fig. 15. Results obtained with the Gough–Stewart robot in Case 1: (a) Desired and realized forces, (b) 3D Cartesian trajectory, (c) Cartesian position errors, (d) Cartesian orientation errors.

UNCORRECTED PROOF

The results obtained with the Orthoglide are presented in Figs. 7 to 10. The choice of the controller gains allows for a smooth transient phase from the unconstrained to the constrained motion (at $t \approx 0.4s$) with zero force steady state error. Figs. 7-a,b, 8-a,b, and 9-a,b show that the force errors are proportional to the accuracy of the vision system: in Case 1, the force error is less than 0.2N on X and Z axis corresponding to the image plane and about 0.4N on Y axis being orthogonal to the image plane oriented along increasing depth. In Case 2, this error is less than 0.1N on X and Z axis and about 0.2N on Y direction. The force errors in Case 3 are about 0.05N on X and Z directions and less than 0.1N on Y direction. These figures show also that the accuracy of the force sensor is less significant: the difference between Cases 2 and 4 can only be observed during the impact phase where the contact force appears more significant in the case 4 (it exceeds 10 N) leading to a more significant position error too. Figs. 7-c and 8-c show that the position control loop is globally not affected by the force control loop either in free or constrained space since the desired and realized trajectories overlap completely. Nevertheless, a residual constant position error is persisting along the force controlled direction (Z axis) after the impact (at $t \approx 0.4s$) which depends on the exerted force and the environment stiffness as it can be observed in Figs. 7-d, 8-d, 9-d and 10-d. This is due to the fact that force control loop is hierarchic upon position control loop along that direction. Cartesian position errors on X and Z axis does not exceed $0.4 \times 10^{-4}m$, $0.15 \times 10^{-4}m$ and $0.05 \times 10^{-4}m$ in Cases 1, 2 and 3 respectively. Whereas, along the Y axis which corresponds to the camera depth, the error is naturally more significant: it reaches $1.2 \times 10^{-4}m$ in Case 1, $0.6 \times 10^{-4}m$ in Case 2 and $0.1 \times 10^{-4}m$ in Case 3. It is very important to notice that the accuracy obtained here in each case can easily be improved by adding more blobs to the observed object to increase the information redundancy. This property constitutes an important advantage of the vision system compared to other pose measurement techniques. No filtering is used to eliminate the measurement noise (force sensor and camera) in this simulation and, as can be seen, the results obtained in Case 2 are rather satisfactory and meet the requirements for highly accurate Q3 applications such as assembly tasks or contour following. The vision system used in Case 1 can be used if one just needs to roughly track a position and force target and low accuracy on force and position tracking is allowed.

The results obtained with the Isoglide are presented in Figs. 11 to 14. Since the obtained results are similar, only errors on force and Cartesian position are shown for the last three cases (subfigures (b) and (d)). The same control performances are maintained using this control scheme: stable contact and normal force regulation is achieved in the four cases with a good trajectory tracking. These results were expected since all dynamics are compensated for in the control law. We observe for this machine also a strong dependence between the vision system performances and the tracking errors values for the two controlled variables (position and contact forces). The accuracy of the force sensor affects the system response essentially in the impact phase.

Please cite this article as: S. Bellakehal, et al., Vision/force control of parallel robots, Mech. Mach. Theory (2011), doi:10.1016/j.mechmachtheory.2011.05.010

The results obtained with the Gough–Stewart robot are presented in Figs. 15 to 17. Good control performances were obtained in general like with the two previous robots and convergence is ensured even if the vision system is roughly calibrated. As it appear in Fig. 15-a (Case 1), the force tracking error is about 0.4N along X and Z axis and less than 0.6N along Y direction corresponding to the camera depth. Since the results on force tracking are similar, force figures are not presented for the other cases. Position errors are about $0.5\times10^{-4}m$ along X and Z axis and less than $1.4\times10^{-4}m$ along Y axis as is depicted in Fig. 15-c. Orientation errors around X and Z axis are about $0.3\times10^{-3}rd$, $0.2\times10^{-3}rd$ and $0.06\times10^{-3}rd$ in Cases 1, 2 and 3 respectively and less than $0.8\times10^{-3}rd$, $0.5\times10^{-3}rd$ and $0.15\times10^{-3}rd$ in Cases 1, 2 and 3 respectively around Y axis (see Figs. 15-d, 17-c and 17d).

Finally, let us note that these results confirm the comparative study between model-based position control and vision-based position control conducted in [30]. It shows indeed the numerous advantages and the superiority of sensor-based control scheme adopted here (Fig. 2) upon model-based control scheme used in [6] (Fig. 1) in the case of parallel machine motion control.

8. Conclusion

Parallel force/vision control for a parallel robot manipulator in contact with plane surface has been derived in this work. To the best of our knowledge, combining force sensing and motion control with high-level guidance from a vision system has not been addressed before for a parallel kinematic machine. Simulation results on the Orthoglide have shown good performance tracking for both contact forces and end-effector motion simultaneously within the proposed control scheme. Tracking errors depends only on sensor performances, namely, the vision system. The same study was conducted on a second parallel robot (the Isoglide-4 T3R1) which has very heavy inertial characteristics compared to the first one (the Orthoglide) and has a different kinematic model. The Isoglide-4 T3R1 has shown similar behavior with respect to the vision system errors variations and the force sensor errors variations. Simulations on a third example of parallel robot, the Gough–Stewart platform, was presented and has shown that the proposed control scheme can easily be applied on different mechanical structures with fully position and orientation capabilities. This result is not surprising since the vision system as an exteroceptive pose measurement is completely independent of the machine kinematics and dynamics and does not make any limitation on the machine geometry.

Using an exteroceptive measure to obtain end-effector pose instead of numerical calculation of the forward kinematic model results in a conceptually elegant sensor-based control scheme which has numerous benefits compared to forward kinematic model-based control. First, it allows for a task space representation for the parallel manipulator dynamics which is

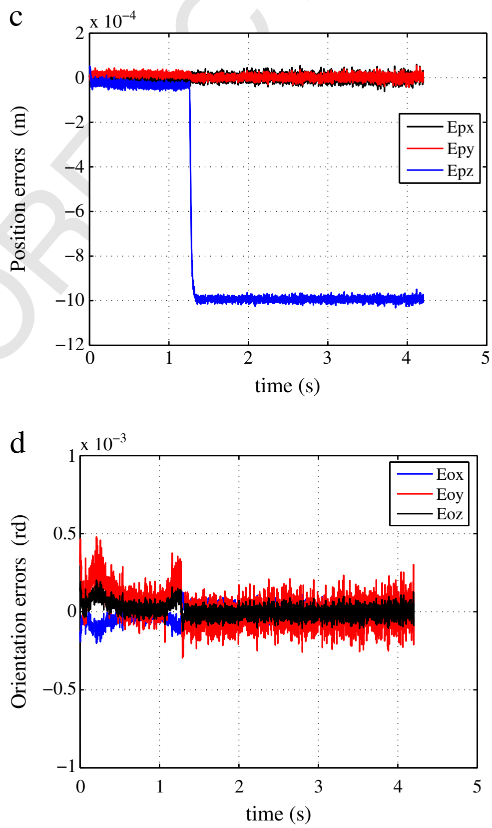

Fig. 16. Results obtained with the Gough–Stewart robot in Case 2: (c) Cartesian position errors, (d) Cartesian orientation errors.

UNCORRECTED PROOF

Please cite this article as: S. Bellakehal, et al., Vision/force control of parallel robots, Mech. Mach. Theory (2011), doi:10.1016/j.mechmachtheory.2011.05.010

ARTICLE IN PRESS

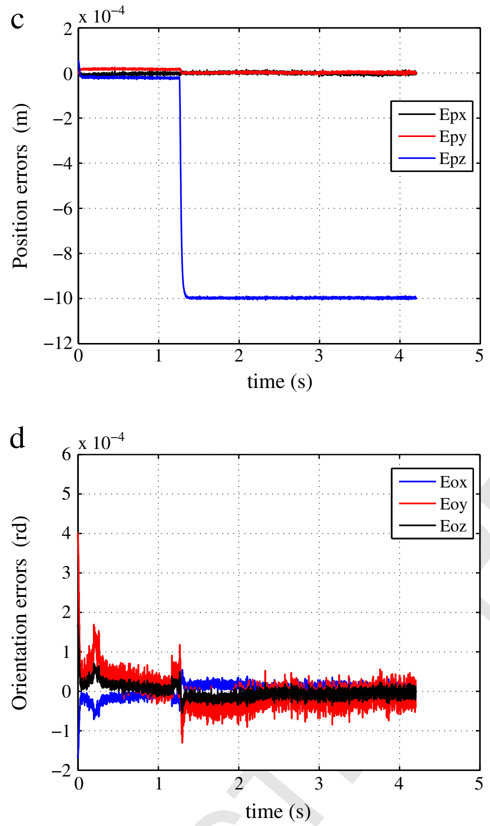

Fig. 17. Results obtained with the Gough–Stewart robot in Case 3: (c) Cartesian position errors, (d) Cartesian orientation errors.

known to be much simpler compared with a joint-space representation. The state feedback control scheme is thus reduced to its simplest expression. Second, it would unburden the control loop from the problems associated with numerical methods of solving a set of nonlinear or polynomial equations, such as local minima, sensitivity to the initial values, finding only one solution, and solutions with imaginary part. Furthermore, the accuracy of the closed-loop performance can be made relatively insensitive to modeling errors such as errors on the machine geometric parameters, encoders errors, errors on the orthogonality of axis, flexion phenomena of links, clearances and assembly defects due to the large number of links and passive joints etc…

Unlike the analytical methods that are restricted to special types of platforms, vision system is a very safe sensor without any contact or physical interaction with the observed scene, so it does not make any restrictions on the geometry, the kinematics or the dynamics of the machine. Additionally, a vision system is very flexible in the sense that depending on the desired level of accuracy and online computation time, the blobs number can be adjusted accordingly. Finally, the obtained results egg on the adoption of vision as a very suitable and promising tool to ensure a precise measure for the end-effector Cartesian pose since computer vision is a field of phenomenal improvement in cameras technology and dedicated hardware for image processing.

Future works will first address the experimental validation of the proposed parallel force/vision control on the studied parallel robots, then, instead of the position servoing by means of visual sensor achieved here, future research efforts will be devoted to extending our approach to an image based visual servoing scheme. The intended scheme consist on regulating the error between the current image and a desired image directly in the image plane since this approach (also named 2D visual servoing) is known as having some degrees of robustness with respect to noise in the image and camera calibration errors.

References

[1] O. Ait-Aider, N. Andreff, P. Martinet, J.-M. Lavest, Simultaneous pose and velocity measurement by vision for high-speed robots, IEEE Int. Conf. on Robotics and Automation (ICRA), May 15–19, 2006, pp. 3742–3747, Orlando, Florida.

[2] Y. Amirat, F. Artigue, J. Pontnau, Force feedback control of a six dof parallel robot: application to assembly in car manufacturing, Revue d'Automatique et de Productique Appliqués 4 (2) (1991) 109–121.

[3] J. Baeten, H. Bruyninckx, J. De Schutter, Integrated vision/force robotic servoing in the task frame formalism, International Journal of Robotics Research 22 (10–11) (Oct-Nov 2003) 941–954.

[4] L.E. Bruzzone, R.M. Molfino, M. Zoppi, Modelling and control of peg-in-hole assembly performed by translational robot, Proc. of the IASTED International Conference on Modelling, Identification and Control, February 18–21, 2002, pp. 512–517, Innsbruck, Austria.
[5] Caccavale, F., Siciliano, B., Villani, L., June 2003. *The tricept robot: Dynamics and impedance control.* 8, (2) 263–268. Q5
[6] M. Callegari, A. Suardi, On the force-controlled assembly operations of a new parallel kinematics manipulator, Proc. of the Mediterranean Conference on Control and Automation, 2003, Rhodes.
[7] S. Chiaverini, L. Sciavicco, The parallel approach to force/position control of robotic manipulators, IEEE Transactions on Robotics and Automation 9 (4) (1993) 361–373.
[8] D. Corbel, O. Company, F. Pierrot, Optimal design of a 6-dof parallel measurement mechanism integrated in a 3-dof parallel machine-tool, IEEE/RSJ International Conference on Intelligent Robots and Systems (IROS), Sep 22–26 2008, Nice, France.
[9] R. Dahmouche, O. Ait-Aider, N. Andreff, Y. Mezouar, High-speed pose and velocity measurement from vision, IEEE Int. Conf. on Robotics and Automation (ICRA), May 19–23, 2008, Pasadena, California.
[10] B. Dasgupta, T.S. Mruthyunjaya, Closed form dynamic equations of the general Stewart platform through the Newton–Euler approach, Mechanism and Machine Theory 33 (7) (1998) 993–1012.
[11] T. De Laet, J. Rutgeerts, W. Decré, R. Smits, E. Aertbeliën, K. Claes, H. Bruyninckx, J. De Schutter, Constraint-based task specification and estimation for sensor-based robot systems in the presence of geometric uncertainty, International Journal of Robotics Research 26 (5) (2007) 433–455.
[12] H. Van Brussel, J. De Schutter, Compliant robot motion II: a control approach based on external control loops, International Journal of Robotics Research 7 (4) (1988) 18–33.
[13] D. Dementhon, L.S. Davis, Model-based object pose in 25 lines of code, International Journal of Computer Vision, Volume 15, 1995, pp. 123–141.
[14] J. DeSchutter, H. Bruynincks, M.W. Spong, Force control: a bird's eye view, IEEE CSS/RAS Int. Workshop on Control Problems in Robotics and Automation: Future Directions, December 1997, San Diego.
[15] E.D. Fasse, C.M. Gosselin, On the spatial impedance control of Gough–Stewart platforms, IEEE Int. Conf. on Robotics and Automation (ICRA), May 1998, pp. 1749–1754, Leuven, Belgium.
[16] P. Fraisse, P. Dauchez, F. Pierrot, Robust force control strategy based on the virtual environment concept, Advanced Robotics, Volume 21, 2007, pp. 485–498.
[17] N. Hogan, Impedance control: an approach to manipulation. Parts I–III, Journal of Dynamic Systems, Measurement and Control 107 (1) (March 1985) 1–24.
[18] C. Huang, L. Liu, X. Wang, S. Shi, Robust scheme of global parallel force/position regulators for robot manipulators under environment uncertainty, Journal of Control Theory and Applications 5 (3) (2007) 271–277.
[19] W. Khalil, S. Guegan, Inverse and direct dynamic modeling of Gough–Stewart robots, IEEE Transaction on Robotics and Automation 20 (4) (2004) 754–762.
[20] W. Khalil, O. Ibrahim, General solution for the dynamic modelling of parallel robots, Journal of Intelligent Robots and Systems 49 (2007) 19–37.
[21] O. Khatib, A unified approach for motion and force control of robot manipulators: the operational space formulation, IEEE Journal of Robotics and Automation, volume 3, Feb 1987, pp. 43–53.
[22] O. Khatib, The operational space framework, JSME International Journal, volume 36, 1993, pp. 277–287.
[23] F. Majou, P. Wenger, D. Chablat, Design of a 3 axis parallel machine tool for high speed machining: the orthoglide, IDMME, May 14–16 2002, Clermont-Ferrand, France.
[24] E. Marchand, F. Chaumette, Virtual Visual Servoing: A Framework for Real-Time Augmented Reality, Volume 21, Blackwell Publishers, 2002.
[25] J.P. Merlet, Force feedback control of parallel manipulators, IEEE Int. Conf. on Robotics and Automation (ICRA), volume 3, April 1988, pp. 1484–1489, Philadelphia, Pennsyvania.
[26] J.P. Merlet, Parallel Robots, Kluwer Academic Publishers, 1999.
[27] G. Morel, E. Malis, S. Boudet, Impedance based combination of visual and force control, IEEE Int. Conf. on Robotics and Automation (ICRA), May 1998, pp. 1743–1748, Leuven, Belgium.
[28] A. Muller, P. Maier, Kinematic and dynamic properties of parallel manipulators, Multibody System Dynamics 5 (3) (2001) 223–249.
[29] B.J. Nelson, J.D. Morrow, P.K. Khosla, Fast stable transitions with a stiff manipulator using force and vision feedback, Int. Conf. on Intelligent Robots and Systems, volume 2, August 1995, pp. 90–95, Pittsburgh,.
[30] F. Paccot, N. Andreff, P. Martinet, A review on the dynamic control of parallel kinematic machines: theory and experiments, International Journal of Robotics Research 28 (3) (2009) 395–416.
[31] F. Paccot, P. Lemoine, N. Andreff, D. Chablat, P. Martinet, A vision-based computed torque control for parallel kinematic machines, IEEE Int. Conf. on Robotics and Automation (ICRA), volume 24, May 19–23 2008, pp. 1556–1561, Pasadena, CA, USA.
[32] A. Pashkevich, D. Chablat, P. Wenger, Kinematics and workspace analysis of a three-axis parallel manipulator: the orthoglide, Robotica, volume 24, 2006, pp. 39–49.
[33] J. Pomares, G.J. Garcia, F. Torres, A robust approach to control robot manipulators by fusing visual and force information, Journal of Intelligent and Robotic Systems 48 (2007) 437–456.
[34] M.H. Raibert, J.J. Craig, Hybrid position force control of manipulators, Journal of Dynamic Systems, Measurement and Control 103 (2) (June 1981) 126–133.
[35] N. Saadia, Y. Amirat, J. Pontnau, R. Cherif, Force feedback control of an assembly robot by neural networks, Int. Conf. on Artificial Neural Networks (ICANN), volume 1327, October 8–10, 1997, Lausanne.
[36] Satya, S.M., Ferreira, P.M., Spong, M.W., 1995 *Hybrid control of a planar 3-dof parallel manipulator for machining operations.* 23, 273–280. Q6
[37] S. Shirai, H. Inoue, Guiding a robot by visual feedback in assembling tasks, Pattern Recognition, volume 5, 1973, pp. 99–108.
[38] B. Siciliano, L. Villani, Robot Force Control, Kluwer, Dordrecht, 2000.
[39] M. Tarokh, Real time forward kinematics solutions for general Stewart platforms, IEEE Int. Conf. on Robotics and Automation (ICRA), April 10–14, 2007, Roma, Italy.
[40] C. Tavolieri, E. Ottaviano, M. Ceccarelli, Pose determination for a rigid body by means of catrasys ii (cassino tracking system), in: Manfred Husty, Hans-Peter Schröcker (Eds.), Proceedings of EuCoMeS, the first European Conference on Mechanism Science, February 21–26 2006, Obergurgl (Austria).
[41] P. Wenger, D. Chablat, Kinematic analysis of a new parallel machine tool: the orthoglide, Advances in Robot Kinematic, 2000, pp. 305–314.

UNCORRECTED PROOF

Please cite this article as: S. Bellakehal, et al., Vision/force control of parallel robots, Mech. Mach. Theory (2011), doi:10.1016/j.mechmachtheory.2011.05.010